





Sensitivity enhancement of nonlinear refractive index measurement by Gaussian-Bessel beam assisted z-scan method

WEI GAO,^{1,2} SANDAN WANG,^{1,2} JINPENG YUAN,^{1,2,3}  LIRONG WANG,^{1,2,4}  LIANTUAN XIAO,^{1,2} AND SUOTANG JIA^{1,2}

¹State Key Laboratory of Quantum Optics and Quantum Optics Devices, Institute of Laser Spectroscopy, Shanxi University, 92 Wucheng Road, Taiyuan 030006, China

²Collaborative Innovation Center of Extreme Optics, Shanxi University, 92 Wucheng Road, Taiyuan 030006, China

³yjp@sxu.edu.cn

⁴wlr@sxu.edu.cn

Abstract: Characterizing the nonlinear optical properties of numerous materials plays a prerequisite role in nonlinear imaging and quantum sensing. Here, we present the evaluation of the nonlinear optical properties of Rb vapor by the Gaussian-Bessel beam assisted z-scan method. Owing to the concentrated energy in the central waist spot and the constant intensity of the beam distribution, the Gaussian-Bessel beam enables enhanced sensitivity for nonlinear refractive index measurement. The nonlinear self-focusing and self-defocusing effects of the Rb vapor are illustrated in the case of blue and red frequency detunings from $5S_{1/2} - 5P_{3/2}$ transition, respectively. The complete images of the evolution of nonlinear optical properties with laser power and frequency detuning are acquired. Furthermore, the nonlinear refractive index n_2 with a large scale of $10^{-6} \text{ cm}^2/\text{W}$ is determined from the measured transmittance peak-to-valley difference of z-scan curves, which is enhanced by a factor of ~ 1.73 compared to the result of an equivalent Gaussian beam. Our research provides an effective method for measuring nonlinear refractive index, which will considerably enrich the application range of nonlinear material.

© 2022 Optica Publishing Group under the terms of the [Optica Open Access Publishing Agreement](#)

1. Introduction

The measurement of nonlinear optical properties is fundamental in the fields of quantum optics [1] and ultrafast optics [2]. In general, nonlinear optical properties are the dependent results of an optical effect on the electric field when a laser interacts with matter [3]. Nonlinear optical properties include mixing [4], frequency doubling [5], linear electro-optic [6] and third-order nonlinear [7]. Until now, the study of nonlinear optical properties has attracted extensive interests for their widespread applications in nonlinear imaging, high-speed optical communications, and all-optical switches [8–11].

The methods for measuring nonlinear optical properties mainly include nonlinear interferometry [12], four-wave mixing [13,14], ellipse rotation [15,16] and beam distortion measurements [17]. Interferometry relies on the precise adjustment of multiple beams to identify the time-resolved moving interference fringes and obtain the nonlinear phase shift of the measured sample. Four-wave mixing, in which three incident light waves interact with atoms to generate a fourth outgoing light, requires a strict experimental condition. Elliptic rotation measurement determines the nonlinear effect of medium by exploring the polarization properties of a laser, which requires complicated wave propagation analysis and has lower measurement sensitivity. The z-scan method, which is based on the spatial beam distortion principle in a single-beam configuration, is a high sensitivity tool for inducing the formation of nonlinear optical properties [18].

The modified z-scan methods, not only can obtain nonlinear optical properties conveniently, but also can provide the high measurement sensitivity of nonlinear coefficients, are always being pursued. It is theoretically proposed that the propagation of Gaussian beams modulated by a Bessel profile can increase the z-scan sensitivity compared with conventional Gaussian beams [19,20]. The initial experimental attempt of the Gaussian-Bessel (GB) beam assisted z-scan method is implemented on organic dyes [21]. The atomic vapor, as a harmless and novel nonlinear optical material, has been used as a robust medium in the field of quantum optics [22–24]. A completely controllable nonlinear optical system can be achieved by understanding the nonlinear optical process evolution of the atomic vapor. Previous research on atomic nonlinear optical properties with Gaussian beam assisted z-scan method shows the strong desire for enhanced sensitivity [25–30]. The GB beam assisted z-scan method provides a powerful tool for the high sensitivity measurement of the nonlinear optical properties of atomic vapors.

In this work, we study the nonlinear optical properties of Rb vapor by GB beam assisted z-scan method. The enhanced self-defocusing and self-focusing effects are observed for red and blue frequency detunings, respectively. The influences of laser power and frequency detuning on the nonlinear optical properties are studied in detail. Finally, the nonlinear refractive index n_2 of the Rb vapor is determined by the peak-to-valley difference ΔT of z-scan curves. The precise measurement of the nonlinear refractive index is of great significance to the exploration of nonlinear materials, which aids in the development of the multi-channel information processing and tunable optical switching.

2. Experimental setup

The experimental setup for studying the nonlinear optical properties of the Rb vapor is demonstrated in Fig. 1(a). The laser is provided by an external cavity diode laser (DL pro, Toptica) with a 780 nm Gaussian beam, which is utilized to excite the $5S_{1/2} - 5P_{3/2}$ transition. The frequency is monitored by a wavelength meter (WS-7, HighFinesse). The reference positions of laser frequency detunings are chosen on the $^{87}\text{Rb } 5S_{1/2}(F = 2) - 5P_{3/2}(F' = 1)$ hyperfine transition for red detunings and $^{85}\text{Rb } 5S_{1/2}(F = 3) - 5P_{3/2}(F' = 4)$ for blue detunings. Meanwhile, the frequency detunings are chosen from 0.7 to 1.5 GHz in the experiment so as to make nonlinear absorption negligible while still possessing an appreciable nonlinear refractive effect. The laser is divided into two beams. One beam is employed as the reference for z-scan measurement with a Gaussian profile. The other beam passes through an axicon (AX) to make the emitted light wave vector symmetrically distributed on the cone by precisely rotation. As a result, the zero-order GB beam is generated by the coherent superposed on the same cone surface. A thin Rb vapor cell, with 1 mm thickness, is placed behind the AX as the measured sample. The temperature of the vapor cell is accurately controlled at 115 °C. And the linear absorption measurement gives an atomic density of $1.51 \times 10^{13} \text{ cm}^{-3}$ [31]. Additionally, a linear translation stage (Thorlabs, LTS300) is employed to precisely control the movement of the vapor cell along the z axis, which has the minimum movement of 0.1 μm and on-axis accuracy of 5 μm . In the far-field, the laser intensity transmittance via the aperture (A) is detected by a photodetector (PD). Furthermore, a charge coupled device (CCD) is also employed to record the transmittance beam profiles. The measurement results of the PD and the CCD both reflect the spatial distortion effect of the laser field simultaneously, which clearly reveals the nonlinear optical response of Rb vapor.

Figure 1(b) shows the transmission schematic diagram of the Gaussian (top) and GB (bottom) beams after passing through a lens (L) and an axicon (AX) on the z axis, respectively. The Gaussian beam diverges rapidly on both sides of the lens focus with strong scattering effect and large energy loss. While, the GB beam maintains excellent non-diffracting property in the Bessel region, which facilitates concentrated energy sources in the central waist spot and a beam distribution with constant intensity [32]. The Bessel region is determined by $z_{max} = \omega_0/\tan \beta$, where ω_0 is the beam waist and β is the deflection angle of the axicon. Therefore, the z-scan

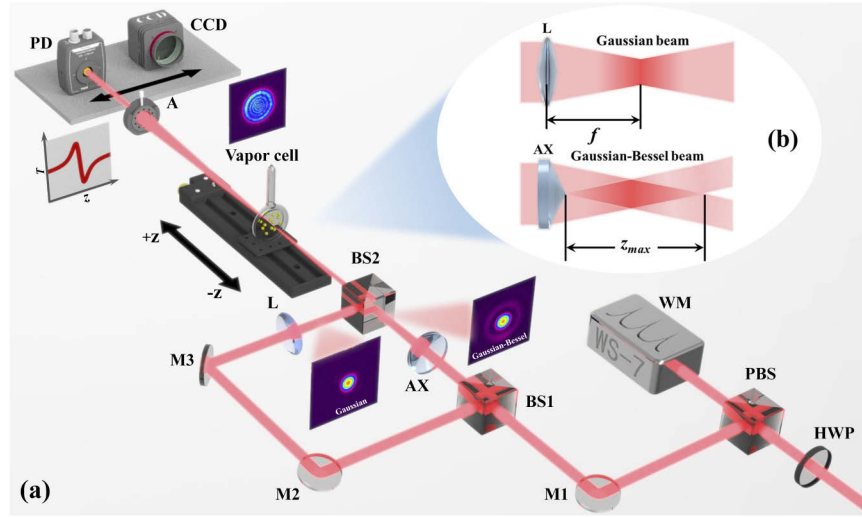


Fig. 1. (a) Sketch of experimental setup. HWP, half-wave plate; PBS, polarization beam splitter; M, high-reflection mirror; BS, beam splitter; L, lens; AX, axicon; A, aperture; PD, photodiode; CCD, charge coupled device; WM, wavelength meter. (b) The transmission schematic diagram of the Gaussian (top) and GB (bottom) beams along the z axis.

method conducted in this region enhances the measurement sensitivity of nonlinear optical properties characterization.

3. Experimental results and discussions

The electric field distribution of the GB beam along the propagation of z direction is represented as [19]:

$$E(z, r, t) = E_0(t) \frac{\omega_0}{\omega(z)} \exp\{i[(k - \zeta^2/2k)z - \Phi(z)]\} J_0[\zeta r/(1 + iz/z_0)] \times \exp\{-1/\omega^2(z) + ik/2R(z)(r^2 + \zeta^2 z^2/k^2)\}, \quad (1)$$

where $E_0(t)$ illustrates the radiation electric field at the focal point, $\omega(z) = \omega_0(1 + z^2/z_0^2)^{1/2}$ is the beam radius at the z position, and $z_0 = k\omega_0^2/2$ is the diffraction length of the beam, $k = 2\pi/\lambda$ is the wave vector, $R(z) = z(1 + z^2/\omega_0^2)$ is the radius of the wavefront curvature at z , φ is the phase of the beam propagating in the medium, $\Phi(z) = \arctan(z/z_0)$ is the phase factor, ζ is the radial wave vector of the GB beam. The beam distribution is dependent on ζ . It is the normal Gaussian beam distribution when ζ^{-1} equals zero.

The influences of nonlinear refraction and diffraction on the laser beam radius are disregarded when the thickness L of the measured sample is less than the diffraction length. The electric field intensity $E_a(r, t)$ at the far-field aperture is obtained using the Gaussian decomposition method and Taylor series expansion $e^{i\Delta\phi(z,r,t)}$ [33]:

$$E_a(r, t) = E(z, r = 0, t) e^{-\alpha L/2} \sum_{m=0}^{\infty} \frac{[i\Delta\phi_0(z, t)]^m}{m!} \frac{\omega_{m_0}}{\omega_m} \exp\left(-\frac{r^2}{\omega_m^2} - \frac{ikr^2}{2R_m} + i\theta_m\right), \quad (2)$$

where $g = 1 + d/R(z)$, d is the distance from the sample to the aperture, $\omega_{m_0}^2 = \omega^2(z)/(2m + 1)$, $R_m = d[1 - \frac{g}{g^2 + d^2/d_m^2}]^{-1}$, $d_m = \frac{k\omega_{m_0}^2}{2}$, $\theta_m = \tan^{-1}[\frac{d/d_m}{g}]$, and $\omega_m^2 = \omega_{m_0}^2[g^2 + \frac{d^2}{d_m^2}]$.

Therefore, the normalized transmittance T of the z-scan method is obtained by [33]:

$$T(z) = \frac{\int_{-\infty}^{+\infty} P_T(\Delta\phi_0(t))dt}{S \int_{-\infty}^{+\infty} P_i(t)dt}, \quad (3)$$

in which $P_T(\Delta\phi_0(t)) = c\varepsilon_0 n_0 \pi \int_0^{r_a} |E_a(r, t)|^2 r dr$, $p_i(t) = \pi\omega_0^2 I_0(t)/2$ is the instantaneous input power, S is the linear transmittance of the far-field aperture, $\Delta\phi_0(t) = kn_2 I_0 L$ is the phase shift at the focal point on the z axis, I_0 is the laser intensity at the focal point, and n_2 is the nonlinear refractive index.

The laser intensity distribution of Gaussian (top) and GB (bottom) beams with the same central beam waist is depicted in Fig. 2(a) by $I = \frac{n\varepsilon_0 c}{2} |E(z, r, t)|^2$, which is also the real situation of our experiment study. It can be found that the laser intensity of the GB beam is slightly smaller than that of the Gaussian beam when there has the same beam waist. While the z-scan normalized transmittance T in the case of Fig. 2(a) is obtained through Eq. (3), which is illustrated in Fig. 2(b). The GB beam transmittance peak-to-valley difference (ΔT) is larger than that of the Gaussian beam, which indicates that the GB beam assisted z-scan method can provide enhanced measurement sensitivity of nonlinear optical properties.

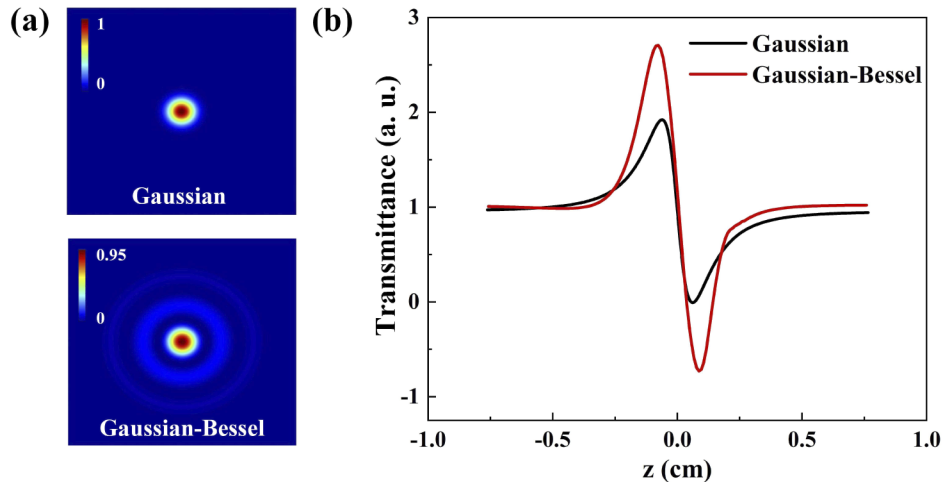


Fig. 2. (a) The laser intensity distribution of Gaussian (top) and GB (bottom) beams with the same central beam waist. (b) The normalized z-scan curves for the Gaussian (black line) and GB (red line) with beams in Fig. 2(a).

The transmitted profiles of GB (top) and Gaussian (bottom) beams after passing through the aperture along different z positions of propagation coordinates are demonstrated in Fig. 3(a) when the laser frequency is red detuning 0.7 GHz. It discovered that the intensity changes as theoretical prediction of strong-weak-strong are observed for both situations of GB and Gaussian beams, which provides a good foundation for the beam spatial distortion principle. The gray dotted boxes from left to right reflect the strongest and weakest positions of the profiles, respectively. Interestingly, the strongest ($z = -0.6$ cm) and the weakest ($z = 0.6$ cm) GB beam distortions are greater than the Gaussian ($z = -0.3$ cm and 0.3 cm) beam. It illustrates that there is a more considerable optical distortion effect of GB beam assisted z-scan method, which has a direct impact on the measurement sensitivity of nonlinear optical properties.

Moreover, the z-scan curves detected by PD with a strong-weak-strong variation trend are reflected clearly, as shown in Fig. 3(b). The dots represent experimental data, while the lines represent theoretical fitting results with Eq. (3). Meanwhile, the z-scan curves illustrate the clear

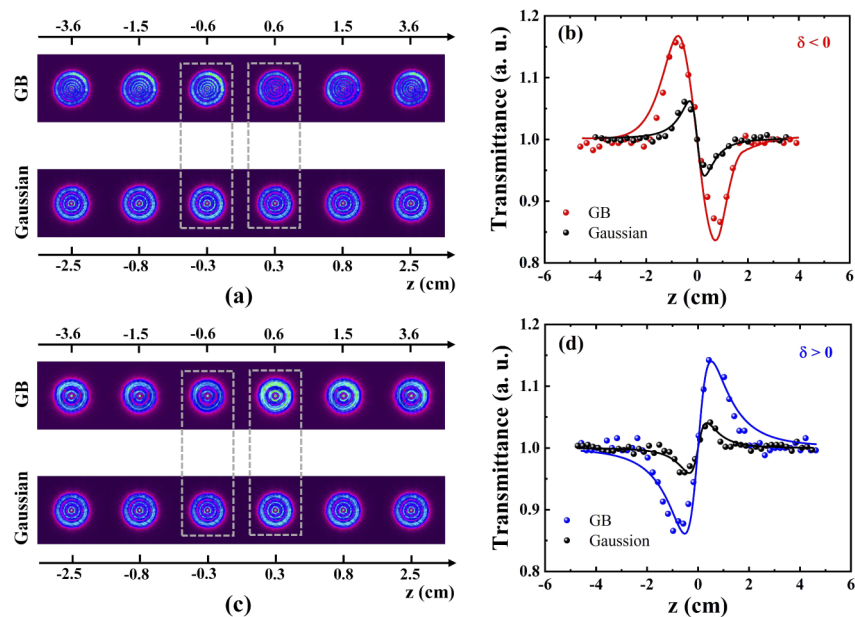


Fig. 3. The transmitted profiles of GB (top) and Gaussian (bottom) beams at different positions along the propagation coordinates for (a) $\delta = -0.7$ GHz and (c) $\delta = 1.3$ GHz, respectively. The gray dotted boxes indicate the strongest and weakest positions of the profiles, respectively. The z-scan curves of Rb vapor for (b) $\delta = -0.7$ GHz and (d) $\delta = 1.3$ GHz in the same experimental conditions of (a) and (c), respectively. The dots represent the experimental data, and the curves denote the theoretical fitting results with Eq. (3).

feature of a pre-focal peak followed by a post-focal valley. The nonlinear refractive index is added to the initial linear refractive index, allowing the Rb vapor to act as a negative lens to the laser beam and exhibit the self-defocusing effect. Additionally, the GB beam assisted z-scan curves have a larger ΔT compared to the Gaussian beam result.

The nonlinear optical properties of blue detuning have similar evolution with red detuning, but with different laws. When the laser frequency is blue detuning 1.3 GHz, the transmitted profiles of GB (top) and Gaussian beam (bottom) are shown in Fig. 3(c). The evolution of transmitted profiles is the inverse of Fig. 3(a), which demonstrates the intensity variation trend of weak-strong-weak. Meanwhile, the z-scan curves depicts a pre-focal valley followed by a post-focal peak as illustrated in Fig. 3(d), indicating a positive nonlinear refractive index corresponding to the self-focusing effect. But the unaltered scenario is the larger ΔT with GB beam compared to the Gaussian beam. Moreover, it can be found that the large frequency detunings lead to small ΔT of z-scan curves by comparing Figs. 3(b) with 3(d), which is consistent with theoretical prediction [34].

The nonlinear optical properties of atomic vapor, as the important nonlinear parameters, can be used to achieve the fully controllable nonlinear optical system in real-time by modifying the experimental conditions. The nonlinear evolution of the Rb vapor is further investigated by adapting the laser intensity and frequency detuning. Figures 4(a) and (b) show the acquired GB beam assisted z-scan curves with different laser powers at 0.7 GHz red detuning and 1.3 GHz blue detuning. The laser power increases from 5 to 21 mW. Clearly, the transmittance peak-to-valley difference ΔT increases with increasing laser power, which attribute to that the significant nonlinear effects of Rb atoms are excited by the high laser intensity. Controllable nonlinear process by changing the laser power enable the adjustment of nonlinear coefficient in all-optical switches [35].

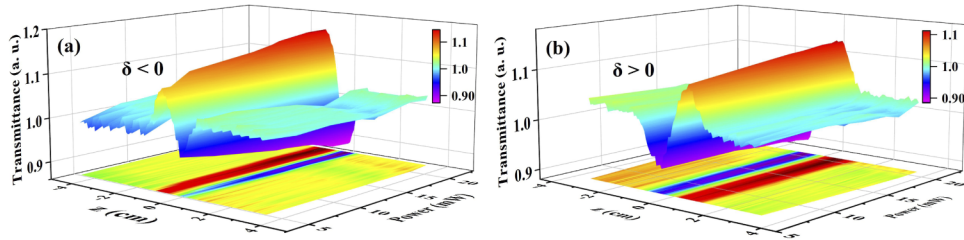


Fig. 4. The GB beam assisted z-scan curves of the Rb vapor versus the laser power when laser frequency (a) $\delta = -0.7$ GHz and (b) $\delta = 1.3$ GHz.

Furthermore, the nonlinear optical properties of Rb vapor are directly affected by laser frequency detunings, which are presented in Fig. 5. The experimental conditions are the same as in Fig. 3 except for frequency detuning. It can be found that the transmittance peak-to-valley difference ΔT decreases when the red frequency detuning increases from 0.7 to 1.5 GHz, which is illustrated in Fig. 5(a). The case of blue frequency detuning (Fig. 5(b)) demonstrates similar behavior. As the frequency detuning increases, the interaction intensity between laser and atoms is weakened, thus, the nonlinear optical effects of the Rb vapor becomes insignificant [36]. The maximum nonlinear effect is acquired at the frequency detuning approximately 0.7 GHz. The high tunability of the nonlinear optical properties by varying laser frequency detuning in Rb atoms makes it an attractive candidate for quantum information processing [37].

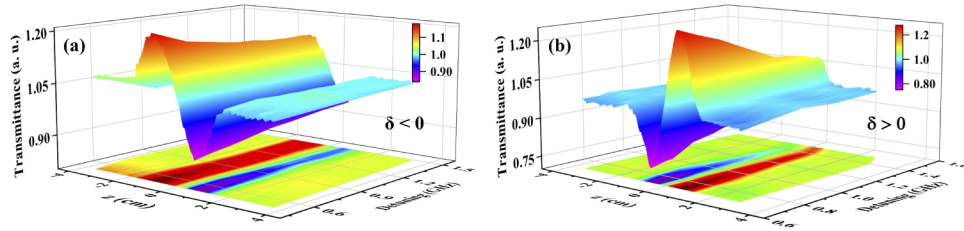


Fig. 5. The GB beam assisted z-scan curves of the Rb vapor versus the red detuning (a) and blue detuning (b) when the laser power is 21 mW.

Finally, the nonlinear refractive index n_2 of the Rb vapor is determined using the ΔT of the GB beam assisted z-scan curves [21]:

$$n_2 = \frac{\Delta T}{0.406[kI_0 \frac{1 - \exp(-\alpha L)}{\alpha}]}, \quad (4)$$

where α is the optical absorption coefficient of the medium. When the input power is 21 mW, the value of $n_{2(GB)}$ is obtained as 2.07×10^{-6} cm²/W with the laser frequency is red detuning 0.7 GHz. Additionally, the $n_{2(G)}$ determined by Gaussian beam in Fig. 3 is 7.58×10^{-7} cm²/W, which is also the limit of the conventional z-scan method [38]. The enhancement rate is characterized as $\kappa = \frac{n_{2(GB)} - n_{2(G)}}{n_{2(G)}}$, therefore the $n_{2(GB)}$ has a factor of ~ 1.73 enhancement. Furthermore, the enhancement effect is guaranteed by GB beam, but the enhancement rate will vary with the employed GB beam mode. Additionally, introducing additional structured light fields, such as flat top beams with the smooth and uniform intensity distribution, also can significantly enhance the measurement sensitivity of nonlinear optical properties with z-scan method.

4. Conclusions

In summary, we study the nonlinear optical properties of Rb vapor using the GB beam assisted z-scan method. Nonlinear self-defocusing and self-focusing effects are acquired with red and blue frequency detuning, respectively. The transmittance peak-to-valley difference ΔT of GB beam assisted z-scan curves is larger than that of Gaussian beam under the same experimental conditions, indicating that the measurement sensitivity is enhanced by using GB beam. Additionally, the direct influences of laser power and frequency detuning on the nonlinear optical effect are observed. As a result, the nonlinear refractive index $n_2 = 2.07 \times 10^{-6} \text{ cm}^2/\text{W}$ is obtained from the measured GB beam assisted z-scan curves, which has a factor of ~ 1.73 enhancement compared to the equivalent Gaussian beam. Not only does our research enable the accurate measurement of the nonlinear refractive index, but it also allows the completely controllable evolution of the nonlinear optical properties, which has potential applications in nonlinear imaging and quantum sensing.

Funding. National Natural Science Foundation of China (61875112, 62075121); The Program for Sanjin Scholars of Shanxi Province; Key Research and Development Program of Shanxi Province for International Cooperation (201803D421034); Shanxi "1331 Project".

Disclosures. The authors declare no conflicts of interest.

Data Availability. Data underlying the results presented in this paper are not publicly available at this time but may be obtained from the authors upon reasonable request.

References

1. P. Jia, Z. Li, Y. Hu, Z. Chen, and J. Xu, "Visualizing a nonlinear response in a Schrödinger Wave," *Phys. Rev. Lett.* **123**(23), 234101 (2019).
2. F. Belli, A. Abdolvand, W. Chang, J. C. Travers, and P. S. Russell, "Vacuum-ultraviolet to infrared supercontinuum in hydrogen-filled photonic crystal fiber," *Optica* **2**(4), 292 (2015).
3. P. A. Franken, A. E. Hill, C. W. Peters, and G. Weinreich, "Generation of optical harmonics," *Phys. Rev. Lett.* **7**(4), 118–119 (1961).
4. B. A. Ko, A. V. Sokolov, M. O. Scully, Z. R. Zhang, and H. W. H. Lee, "Enhanced four-wave mixing process near the excitonic resonances of bulk MoS₂," *Photonics Res.* **7**(3), 251 (2019).
5. A. R. Tunyagi, M. Ulex, and K. Betzler, "Noncollinear optical frequency doubling in strontium barium niobate," *Phys. Rev. Lett.* **90**(24), 243901 (2003).
6. S. Yang and D. Liu, "Phase compensation method in OPA system based on the linear electro-optic effect," *Photonics* **8**(4), 126 (2021).
7. J. Yuan, C. Wu, L. Wang, G. Chen, and S. Jia, "Observation of diffraction pattern in two-dimensional optically induced atomic lattice," *Opt. Lett.* **44**(17), 4123 (2019).
8. J. N. Potter, A. J. Croxford, and P. D. Wilcox, "Nonlinear ultrasonic phased array imaging," *Phys. Rev. Lett.* **113**(14), 144301 (2014).
9. K. Tsujino, D. Fukuda, G. Fujii, S. Inoue, M. Fujiwara, M. Takeoka, and M. Sasaki, "Quantum receiver beyond the standard quantum limit of coherent optical communication," *Phys. Rev. Lett.* **106**(25), 250503 (2011).
10. J. Sheng, U. Khadka, and M. Xiao, "Realization of all-optical multistate switching in an atomic coherent medium," *Phys. Rev. Lett.* **109**(22), 223906 (2012).
11. J. Yuan, H. Zhang, C. Wu, L. Wang, L. Xiao, and S. Jia, "Tunable optical vortex array in a two-dimensional electromagnetically induced atomic lattice," *Opt. Lett.* **46**(17), 4184 (2021).
12. J. Chandezon, J.-M. Rampnoux, S. Dilhaire, B. Audoin, and Y. Guillet, "In-line femtosecond common-path interferometer in reflection mode," *Opt. Express* **23**(21), 27011 (2015).
13. Y. Kitagawa, R. L. Savage, and C. Joshi, "Demonstration of collisionally enhanced degenerate four-wave mixing in a plasma," *Phys. Rev. Lett.* **62**(2), 151–154 (1989).
14. J. J. Pigeon, S. Ya. Tochitsky, E. C. Welch, and C. Joshi, "Measurements of the nonlinear refractive index of air, N₂, and O₂ at 10 μm using four-wave mixing," *Opt. Lett.* **41**(17), 3924 (2016).
15. J. A. C. Gomes, E. C. Barbano, and L. Misoguti, "Cross-section profile of the nonlinear refractive index of Gorilla Glass obtained by nonlinear ellipse rotation measurements," *Appl. Opt.* **58**(28), 7858 (2019).
16. L. Misoguti, L. R. P. Kassab, C. D. S. Bordon, J. J. Rodrigues, and M. A. R. C. Alencar, "Nonlinear refraction and absorption spectroscopy of tellurite glasses within telecom bands," *J. Alloys Compd.* **872**, 159738 (2021).
17. R. de Nalda, R. del Coso, J. Requejo-Isidro, J. Olivares, A. Suarez-Garcia, J. Solis, and C. N. Afonso, "Limits to the determination of the nonlinear refractive index by the z-scan method," *J. Opt. Soc. Am. B* **19**(2), 289 (2002).
18. M. Sheik-bahae, A. A. Said, and E. W. Van Stryland, "High-sensitivity, single-beam n_2 measurements," *Opt. Lett.* **14**(17), 955 (1989).

19. S. Hughes and J. M. Burzler, "Theory of z-scan measurements using Gaussian-Bessel beams," *Phys. Rev. A* **56**(2), R1103–R1106 (1997).
20. X. Jin, M. Shui, Y. X. Wang, C. W. Li, J. Y. Yang, X. R. Zhang, K. Yang, and Y. L. Song, "Theory of Z-scan technique using Gaussian Bessel beams with a phase object," *Chin. Phys. B* **19**(7), 074203 (2010).
21. M. M. M. Otero, M. L. A. Carrasco, M. D. I. Castillo, G. C. M. Jiménez, and F. R. García, "Experimental z-scan measurements using Gaussian-Bessel beams," *AIP Conf. Proc.* **992**, 559–564 (2008).
22. H. Cai, J. Liu, J. Wu, Y. He, S.-Y. Zhu, J.-X. Zhang, and D.-W. Wang, "Experimental observation of momentum-space chiral edge currents in room-temperature atoms," *Phys. Rev. Lett.* **122**(2), 023601 (2019).
23. Z. Zhang, S. Liang, F. Li, S. Ning, Y. Li, G. Malpuech, Y. Zhang, M. Xiao, and D. Solnyshkov, "Spin-orbit coupling in photonic graphene," *Optica* **7**(5), 455 (2020).
24. Z. Zhang, R. Wang, Y. Zhang, Y. V. Kartashov, F. Li, H. Zhong, H. Guan, K. Gao, F. Li, Y. Zhang, and M. Xiao, "Observation of edge solitons in photonic graphene," *Nat. Commun.* **11**(1), 1902 (2020).
25. S. Sinha, G. K. Bhowmick, S. Kundu, S. Sasikumar, S. K. S. Nair, T. B. Pal, A. K. Ray, and K. Dasgupta, "A z-scan study of nonlinear refraction in sodium vapor," *Opt. Commun.* **203**(3-6), 427–434 (2002).
26. C. F. McCormick, D. R. Solli, R. Y. Chiao, and J. M. Hickmann, "Nonlinear absorption and refraction in near-detuned rubidium vapor," *J. Opt. Soc. Am. B* **20**(12), 2480 (2003).
27. L. Y. Pei, "Enhanced third-order nonlinear processes based on Raman resonance," *Acta Phys. Sin.* **69**(16), 164203 (2020).
28. S. Wang, J. Yuan, L. Wang, L. Xiao, and S. Jia, "Measurement of the Kerr nonlinear refractive index of the Rb vapor based on an optical frequency comb using the z-scan method," *Opt. Express* **28**(25), 38334 (2020).
29. M. O. Araujo, H. L. D. de S. Cavalcante, M. Oria, M. Chevrollier, and T. P. de Silans, "Measurement of the Kerr nonlinear refractive index of Cs vapor," *Phys. Rev. A* **88**(6), 063818 (2013).
30. F. C. Dias Dos Santos, J. C. De Aquino Carvalho, G. T. Moura, and T. Passreat De Silans, "Measurement of the nonlinear refractive index of Cs D1 line using z-scan," *J. Opt. Soc. Am. B* **36**(9), 2468 (2019).
31. A. Sargsyan, A. Amiryan, Y. Pashayan-Leroy, C. Leroy, A. Papoyan, and D. Sarkisyan, "Approach to quantitative spectroscopy of atomic vapor in optical nanocells," *Opt. Lett.* **44**(22), 5533 (2019).
32. Q. Zhang, X. Cheng, H. Chen, B. He, Z. Ren, Y. Zhang, and J. Bai, "Enhancement of phase conjugation degenerate four-wave mixing using a Bessel beam," *Photonics Res.* **6**(3), 162 (2018).
33. M. Sheik-bahae, A. A. Said, T.-H. Wei, D. J. Hagan, and E. W. Van Stryland, "Sensitive measurement of optical nonlinearities using a single beam," *IEEE J. Quantum Electron.* **26**(4), 760–769 (1990).
34. D. Grischkowsky and J. A. Armstrong, "Self-defocusing of light by adiabatic following in rubidium vapor," *Phys. Rev. A* **6**(4), 1566–1570 (1972).
35. H. Wang, D. Goorskey, and M. Xiao, "Enhanced Kerr nonlinearity via atomic coherence in a three-level atomic system," *Phys. Rev. Lett.* **87**(7), 073601 (2001).
36. X. Cheng, Q. Zhang, H. Chen, B. He, Z. Ren, Y. Zhang, and J. Bai, "Demonstration of Bessel-like beam with variable parameters generated using cross-phase modulation," *Opt. Express* **25**(21), 25257 (2017).
37. J. Yuan, S. Dong, C. Wu, L. Wang, L. Xiao, and S. Jia, "Optically tunable grating in a V + Ξ configuration involving a Rydberg state," *Opt. Express* **28**(16), 23820 (2020).
38. C. F. McCormick, D. R. Solli, R. Y. Chiao, and J. M. Hickmann, "Saturable nonlinear refraction in hot atomic vapor," *Phys. Rev. A* **69**(2), 023804 (2004).